IEEE *Access*
Multidisciplinary ⋮ Rapid Review ⋮ Open Access Journal

Impact of Mutual Coupling on Power-Domain Non-Orthogonal Multiple Access (NOMA)

NANN WIN MOE THET [1], SANA KHAN[1], ERCUMENT ARVAS[2], (Life Fellow, IEEE), AND MEHMET KEMAL OZDEMIR[2]
[1]Graduate School of Engineering and Natural Sciences, Istanbul Medipol University, Istanbul, Turkey
[2]School of Engineering and Natural Sciences, Istanbul Medipol University, Istanbul, Turkey

Corresponding author: Nann Win Moe Thet (e-mail: nthet@st.medipol.edu.tr).

ABSTRACT This paper investigates the impact of mutual coupling (MC) on the achievable sum-rate of power-domain non-orthogonal multiple access (NOMA) system in both uplink (UL) and downlink (DL) transmissions. We assume a single-antenna user NOMA system with directional beamforming in the millimeter wave (mmW) channel. Due to the electromagnetic interaction between the antenna elements, called mutual coupling, at the base station (BS), the steering vector of the channel is affected. Consequently, this leads to distorted antenna pattern pointing towards different directions and reduction in channel gain, based on antenna array structure. In this paper, different antenna geometries and configurations, such as one-dimensional (1D) uniform linear array (ULA), two-dimensional (2D), and three-dimensional (3D) uniform circular array (UCA), are implemented at the BS, where induced electromotive force (EMF) and method of moment (MOM) techniques are used to generate the MC coefficients. We first examine the antenna patterns affected by MC, followed by channel gains of user terminals (UT)s. Then sum-rate of the NOMA system is modified in the presence of MC. Furthermore, mutual coupling is compensated successfully for both UL and DL systems for the given antenna structures. Simulation results show that mutual coupling degrades the sum-rate performance of the NOMA system in all three array structures, especially in the UCA structure due to the smaller spacing of the array element in a circular shape, resulting in symmetric mutual coupling from both sides of the circle. On the other hand, it is also shown that compensating the mutual coupling effect by the MOM technique in the case of unknown MC or matrix inversion in the case of known MC significantly improves the system sum-rate in all scenarios.

INDEX TERMS Non-orthogonal multiple access (NOMA), multi-user beamforming, millimeter wave, sum-rate, mutual coupling (MC), uniform linear array (ULA), uniform circular array (UCA), 3D UCA.

I. INTRODUCTION

With the rapid growth of the demand in wireless communications services and scarcity in the frequency spectrum, non-orthogonal multiple access (NOMA) has been gaining attention over the past few years. Compared to orthogonal multiple access (OMA) technology, in power-domain NOMA, multiple users can be served at the same frequency and time, using different allocated power levels at the users. This then provides higher spectral efficiency and more number of users [1], [2]. This distinctive characteristic of NOMA is achieved by employing successive interference cancellation (SIC) technique, which was first introduced in [3]. In downlink (DL)

NOMA, the users with strong channel gain can perfectly cancel the interference from weak users using SIC before decoding its own signal [4], [5]. On the contrary, in uplink (UL) NOMA, far users with the weak channel condition can remove the strong user interference via SIC since all users can utilize the maximum power available at them [4], [6].

The applications of millimeter wave (mmWave) communication have become the essential technology for Fifth-Generation (5G) and beyond wireless communications systems [7], [8]. Thus, many researchers have been paying attention to the research where NOMA system is integrated with multiple-antenna beamforming techniques in mmWave

channel [9]–[13]. By exploiting the degree of freedom in spatial-domain in addition to the advantage of NOMA, groups of users can be supported by NOMA spatially in different beams [5], [6]. However, in practical transmission, mutual coupling (MC) between antenna array elements causes performance degradation of the overall system such as changes in the radiation pattern of the array, input impedance, gain, and bandwidth. Moreover, there exists a system sum-rate degradation if a properly compensated beamforming is not adopted [14], [15]. Therefore, mutual coupling, which can be obtained using different estimation methods [16]–[20], must be compensated to reduce its adverse effect on the system. In the case where MC coefficients cannot be estimated perfectly, different MC compensation techniques, which include invasive and non-invasive techniques, can be used to compensate for the performance degradation. However, invasive techniques result in the complexity of the system due to physical modification of the antenna array structure [21].

A. MOTIVATION AND CONTRIBUTIONS

There have been a number of studies which extensively investigate the mutual coupling effect on the performance of conventional multiple-input multiple-output (MIMO) systems with different antenna structures, mostly uniform linear array (ULA), uniform circular array (UCA), and uniform rectangular array (URA) [14], [15], [22]–[26]. In the studies of [27], [28], the authors also consider concentric circular antenna array (CCAA), where many concentric circular rings with different radii are placed in XY-plane. They formulated the mutual coupling based on method-of-moments (MOM) and induced electromotive force (EMF) [29], respectively. The study in [24] discussed the effect of mutual coupling and transmit correlation in basic two-user MIMO without considering beamforming. On the other hand, in [14], the author considered uplink multiuser large-scale MIMO system with URA and examined the effect of MC on the sum-rate performance using the optimal beamforming vector. It is worth noticing that most of the studies in the array processing depend on the closed-form mutual coupling formula generated by the induced EMF method.

Based on the above-mentioned literature, it is observed that the study on the mutual coupling formulation specifically in three-dimensional (3D) UCA structure, where several UCAs with different radii are placed above each other, is still limited. Moreover, to the best of the authors' knowledge, there is no existing study in the literature that focuses on the mutual coupling effect in multi-antenna NOMA system. Motivated by the aforementioned reasons, in this paper, we investigate the performance of DL and UL NOMA systems in the presence of mutual coupling based on different antenna array configurations. We utilize non-invasive technique for compensation of mutual coupling for both DL [30] and UL [31] transmissions. The followings summarize the main contributions of the paper:

1) Formulation of mutual coupling matrix (MCM) based on induced EMF method in one-dimensional (1D)

ULA, two-dimensional (2D) UCA and staggered 3D UCA structure is discussed.
2) The antenna beam patterns affected by mutual coupling are presented based on the above-mentioned array structures, using both MOM electromagnetic (EM) simulation and induced EMF closed-form formula.
3) The effect of mutual coupling on channel gain of the K numbers of UTs is examined, then the modified achievable sum-rate of NOMA system in the presence of mutual coupling is derived.
4) Mutual coupling is compensated for both DL and UL transmissions, and numerical results on the achievable sum-rate of NOMA system are analyzed and compared to that of the coupled system, employing three different antenna array structure mentioned above.

B. ORGANIZATION AND NOTATION

The rest of the paper is organized as follows. We present the system model that includes the channel model and array geometries in Section II. In Section III, NOMA signal models and their respective achievable sum-rates are elaborated. The effect of MC on the sum-rate of NOMA system is formulated, along with the MC compensation techniques, in Section IV. Numerical results are discussed in Section V, followed by conclusion remarks in Section VI.

We use the following notation throughout this paper: A bold uncapitalized letter, a, means a vector, and a bold capitalized letter, A, means a matrix. $a \in C^{N \times 1}$ stands for complex-valued vector a with size $N \times 1$. I_N denotes an $N \times N$ identity matrix. $(\cdot)^T$ and $(\cdot)^H$ represent transpose and Hermitian (conjugate transpose) operators, respectively. $\sim \mathcal{CN}(a, b)$ denotes circularly symmetric complex Gaussian distribution with mean a and variance b, and $\sim \mathcal{U}(c, d)$ means uniform distribution between c and d bounds. $tr(\cdot)$ denotes trace of a matrix. Toeplitz(A, A) and blkdiag(A, A) stand for symmetric Toeplitz matrix and block diagonal matrix of a matrix A, respectively. $||A||_F$ represents the Frobenius norm of the matrix A and $|(\cdot)|$ means absolute value.

II. SYSTEM MODEL

In this section, we describe the power domain NOMA in both DL and UL systems. Consider a single-cell multiple-input single–output (MISO)-NOMA system where a base station (BS) is equipped with uniform array either ULA or UCA consisting of N antenna elements as depicted in Fig. 1. The BS serves K single-antenna user terminals (UT)s and the perfect channel state information (CSI) is assumed to be known at the BS. The details of the channel model and the signal models in both DL and UL are elaborated in the following subsections.

A. CHANNEL MODEL

A directional mmWave channel based on geometric model is adopted, where only line-of-sight (LOS) channel is considered due to its channel gain dominant over non-line-of-sight
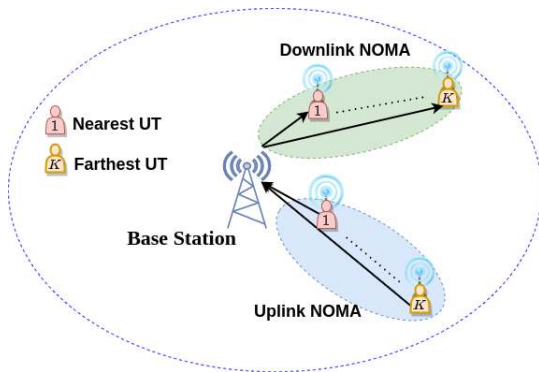
FIGURE 1. MISO-NOMA system model, where BS serves K NOMA-UTs.

(a) 3D view.   (b) Top view.

FIGURE 2. Uniform circular array geometry: (a) 3D view, (b) Top view in XY-plane.

(NLOS) channel gain [32], [33]. The UL mmWave channel vector between the BS and the kth UT, is defined as

$$\boldsymbol{h}_{ULk} = \sqrt{\frac{N}{\rho_k}}\alpha_k \boldsymbol{a}(\phi_k, \theta_k) \in C^{N \times 1}, \qquad (1)$$

where $\rho_k = (4\pi/\lambda)^2 d_k^\eta$ is the path-loss (PL) between the BS and user k with the distance d_k and the PL exponent η at λ transmission wavelength, and $\alpha_k \sim \mathcal{CN}(0, 1)$ denotes the complex gain of the path. $\boldsymbol{a}(\phi_k, \theta_k) \in C^{N \times 1}$ is an antenna array steering vector, based on the array geometry such as ULA, UCA, etc. ϕ_k and θ_k are the azimuth and elevation angles of the direction-of-arrival (DoA)/ direction-of-departure (DoD), respectively. Assuming a reciprocal channel, the DL channel vector between the UTs and the BS can be expressed as $\boldsymbol{h}_{DLk} = \boldsymbol{h}_{ULk}^H \in C^{1 \times N}$. In the subsequent sections of this paper, we omit the subscripts "DL/UL" in the channel vector, and only use $\boldsymbol{h}_k = \boldsymbol{h}_{ULk}$ for the sake of readability.

B. ARRAY STEERING VECTOR

Consider a BS with 1D ULA along the y-axis with inter-element spacing $d = \lambda/2$, the normalized steering vector with elevation angle fixed at $\theta_k = \pi/2$ and the first antenna element placed at the origin, is given by

$$\boldsymbol{a}_k(\phi_k, \theta_k) = \frac{1}{\sqrt{N}} e^{j\beta dn \sin\theta_k \sin\phi_k}, n = [0, \dots, N-1]^T, \quad (2)$$

where $\beta = 2\pi/\lambda$, and signal of the kth UT is transceived at the azimuth angles, $\phi_k \sim \mathcal{U}(-\pi, \pi)$. In case of a UCA with radius, r, which lies in the XY-plane as shown in Fig. 2, the steering vector with $\theta_k = \pi/2$ can be written as

$$\boldsymbol{a}_k(\phi_k, \theta_k) = \frac{1}{\sqrt{N}} e^{j\beta r \sin\theta_k \cos(\phi_k - \phi_n)}, \qquad (3)$$

where $\phi_n = 2\pi n/N_t$ is the angular position of the $n = [1, \dots, N]^T$ antenna elements.

Another array geometry considered in this study is a staggered 3D UCA array structure. As illustrated in Fig. 3, the inner UCA (1st circle) with the radius, r_1, and the size, N_1, is placed above the outer UCA (2nd circle) with the radius, r_2,
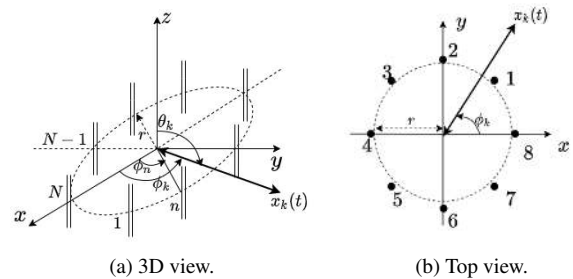
and the size, N_2, at $z = \lambda/4$ on the z-axis. The steering vector in this case can be obtained by concatenating the steering vectors of inner and outer UCA. The steering vector of the 1st UCA for the kth UT is given as

$$\boldsymbol{a}_k^{(1)}(\phi_k, \theta_k) = \frac{1}{\sqrt{N}} e^{j\beta(r \sin\theta_k \cos(\phi_k - \phi_n) + z \cos\theta_k)}. \qquad (4)$$

Considering $\theta_k = \pi/2$, (4) is reduced to the steering vector of non-staggered UCA as (3), and the steering vector of the 2nd UCA, $\boldsymbol{a}_k^{(2)}(\phi_k, \theta_k)$, is given as the same in (3). Without loss of generality, steering vector of 3D UCA with H circles in general is written as

$$\boldsymbol{a}_k(\phi_k, \theta_k) = \left[\boldsymbol{a}_k^{(1)}(\phi_k, \theta_k)^T, \dots, \boldsymbol{a}_k^{(H)}(\phi_k, \theta_k)^T \right]^T. \qquad (5)$$

It can be seen that the steering vector is largely based on the

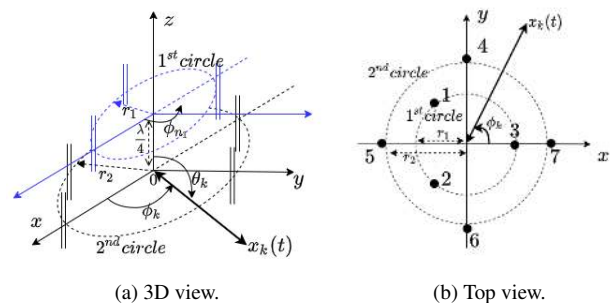(a) 3D view.   (b) Top view.

FIGURE 3. Uniform circular array geometry with staggered UCA at $z = \lambda/4$: (a) 3D view, (b) Top view in XY-plane.

array geometries, number of array element, and inter-element spacing. Depending on the configuration, the beam pattern and the radiated power are affected. In the following section, the background on NOMA signal models for downlink and uplink transmission will be described, along with the respective achievable sum-rates will be investigated.

III. SIGNAL MODEL AND ACHIEVABLE SUM-RATE

In this section, we present the NOMA signal models for downlink and uplink transmissions and their achievable system sum-rates. In ULA and 2D UCA, we assume that K UTs are selected to be served using NOMA for a given time, and each user transmits only one data stream. We consider that the first UT, $k = 1$, is the nearest user to the BS, followed

by UTs $k = 2, \ldots, K$. With perfect CSI given at the BS, we use phased array analog beamforming/combining vectors based on the nearest UT as $v = f = a_1(\phi_1)$, respectively. In 3D UCA, 4 clusters of two-UTs are assumed by using hybrid beamforming with 4 radio-frequency (RF) chains at the BS.

A. DOWNLINK NOMA TRANSMISSION

In downlink NOMA transmission, by using a directional beamforming vector v in the same frequency band, a BS transmits a superimposed data stream $x = \sum_{k=1}^{K} \sqrt{p_k} s_k$ to K UTs, where $s_k; \forall k = 1, 2, \ldots, K$, is the data symbol of the UT k. The received signal at k^{th} UT, where the effective channel gain has the following order; $|h_1^H v|^2 > |h_2^H v|^2 > \cdots > |h_K^H v|^2$, is expressed as

$$y_k = h_k^H v x + w_k, \qquad (6)$$

$$= \underbrace{h_k^H v \sqrt{p_k} s_k}_{\text{Desired signal}} + \underbrace{\sum_{k'=1, k' \neq k}^{K} h_k^H v \sqrt{p_{k'}} s_{k'}}_{\text{Interference from other users}} + w_k, \qquad (7)$$

where $v = [v_1, \ldots, v_N]^T \in \mathbb{C}^{N \times 1}$ is the normalized transmit beamforming vector, also known as excitation voltages. $w_k \sim \mathcal{CN}(0, \sigma_k^2) \in \mathbb{C}^{K \times 1}$ is the additive white Gaussian noise (AWGN) with zero-mean and σ_k^2-variance. $p_k = \gamma_k P_t$ is the allocated power of the user k, using the power allocation coefficients, γ_k with $\sum_{k=1}^{K} \gamma_k = 1$, and P_t is total transmission power.

In order to perfectly decode the desired signal without interference at the nearer UTs, SIC technique, which requires different power allocation as $\gamma_1 < \gamma_2 < \cdots < \gamma_K$ such that lower power values are allocated at the nearer UTs, is applied. Taking advantage of the SIC technique, the UTs located nearer to the BS, which have the stronger channel gain, can successively decode and cancel the signals from the weaker UTs. Therefore, the farthest or cell-edge UT directly decodes the received signal without SIC, hence, there is interference from all of the nearer UTs [2], [34]. Thus, the achievable sum-rate of the nearest UT, without interference, and the rest of the UTs, with other users interference, are defined as

$$R_1^{DL} = \log_2\left(1 + \frac{|h_1^H v|^2 \gamma_1 P_t}{\sigma_1^2}\right), \qquad (8)$$

$$R_{k=2, \ldots, K}^{DL} = \log_2\left(1 + \frac{|h_k^H v|^2 \gamma_k P_t}{|h_k^H v|^2 \sum_{k'=1}^{k-1} \gamma_{k'} P_t + \sigma_k^2}\right). \qquad (9)$$

B. UPLINK NOMA TRANSMISSION

In uplink NOMA system, signals s_k from $k = 1, 2, \ldots, K$ UTs are transmitted simultaneously at the same time and frequency to the BS via their respective channel. The superimposed received signal vector at the BS, $y \in \mathbb{C}^{N \times 1}$, is given by

$$y = \sum_{k=1}^{K} h_k \sqrt{p_k} s_k + w, \qquad (10)$$

where w is the AWGN vector at the BS. Unlike DL NOMA, there is no power allocation constraint in UL NOMA since the UTs can utilize maximum power available to them. The received signal of kth UT at the BS after post-coding with the combiner vector $f \in \mathbb{C}^{N \times 1}$ is written by

$$r_k = \underbrace{f^H h_k \sqrt{p_k} s_k}_{\text{Desired signal}} + \underbrace{\sum_{k'=1, k' \neq k}^{K} f^H h_{k'} \sqrt{p_{k'}} s_{k'}}_{\text{Interference from other users}} + f^H w. \qquad (11)$$

Here, since the received signal at the nearest UT is decoded without employing SIC due to its highest received power, the interference from the far UTs cannot be removed, while SIC is applied at the far UTs successively to remove the interference from the nearer UTs. Thus, the achievable sum-rates of the farthest cell-edge UT K, without interference, and the remaining UTs can be expressed by

$$R_K^{UL} = \log_2\left(1 + \frac{|f^H h_K|^2 \gamma_K P_t}{\sigma_K^2}\right), \qquad (12)$$

$$R_{k=1, \ldots, K-1}^{UL} = \log_2\left(1 + \frac{|f^H h_k|^2 \gamma_k P_t}{\sum_{k'=k+1}^{K} |f^H h_{k'}|^2 \gamma_{k'} P_t + \sigma_k^2}\right). \qquad (13)$$

In the presence of analog beamforming/combining vector $v = f = a(\phi_1)$, the maximum array radiated power for k^{th} UT at the BS in XY-plane can be expressed by (14) and (15)

$$\zeta^{DL}(\phi_k) = |a(\phi_k)^H v|^2 = |a(\phi_k)^H a(\phi_1)|^2, \qquad (14)$$

$$\zeta^{UL}(\phi_k) = |f^H a(\phi_k)|^2 = |a(\phi_1)^H a(\phi_k)|^2. \qquad (15)$$

In the next section, the effect of mutual coupling on the achievable sum-rate of the NOMA based on different antenna array structure will be explored.

IV. MUTUAL COUPLING EFFECT ON THE ACHIEVABLE SUM-RATE

In practice, electromagnetic interaction between the antenna array elements, known as mutual coupling, occurs in any array geometries and affects the steering vector. Consequently, the transmit antenna beam pattern is no longer directed towards the desired user direction. In the following subsections the background on mutual coupling matrix, the practical array pattern due to mutual coupling, and its effect on the achievable sum-rate of the NOMA system will be discussed. Afterward, a solution to this problem in the form of mutual coupling compensation will be presented. Three different radiation patterns are shown; *theoretical pattern* based on the pattern multiplication method that assumes no mutual coupling, *practical pattern* that includes the effect of mutual coupling, and *compensated pattern* that is the pattern after mutual coupling has been compensated for the array structure.

A. MUTUAL COUPLING MATRIX (MCM) BASED ON ARRAY CONFIGURATION

The effective steering vectors and the coupled channel vectors of the UT k in UL and DL transmissions, are respectively written by [14], [15], [26]

$$\hat{a}_k^{UL}(\phi_k) = \boldsymbol{C}\boldsymbol{a}_k(\phi_k) \in \mathbb{C}^{N \times 1}, \tag{16}$$

$$\hat{a}_k^{DL}(\phi_k) = (\boldsymbol{C}\boldsymbol{a}_k(\phi_k))^H = \boldsymbol{a}_k(\phi_k)^H \boldsymbol{C}^H \in \mathbb{C}^{1 \times N}, \tag{17}$$

$$\hat{h}_k^{UL} = \boldsymbol{C}\boldsymbol{h}_k = \sqrt{\frac{N}{\rho_k}}\alpha_k \boldsymbol{C}\boldsymbol{a}(\phi_k) \in C^{N \times 1}, \tag{18}$$

$$\hat{h}_k^{DL} = (\boldsymbol{C}\boldsymbol{h}_k)^H = \sqrt{\frac{N}{\rho_k}}\alpha_k \boldsymbol{a}^H(\phi_k) \boldsymbol{C}^H \in C^{1 \times N}, \tag{19}$$

where $\boldsymbol{C} \in \mathbb{C}^{N \times N}$ denotes MCM, and it can be defined as [35], [36]

$$\boldsymbol{C} = (Z_A + Z_L)(\boldsymbol{Z} + Z_L \boldsymbol{I}_N)^{-1}, \tag{20}$$

where Z_A is the self impedance (isolated impedance), which is $Z_A = (73 + j42.5)\ \Omega$ for half-wavelength dipole antenna with length $l = \lambda/2$, and $Z_L = 50\ \Omega$ is the terminal impedance connected to each antenna element. $\boldsymbol{Z} \in C^{N \times N}$ is the mutual impedance matrix of the array, where its diagonal elements are the same as the self impedance, $Z_{mn} = Z_A, \forall m = n$. The mutual impedance between m^{th} and n^{th} equal length half-wavelength dipole antennae can be written as $Z_{mn} = R_{mn} + jX_{mn}$, where R_{mn} and X_{mn} are the resistance and the reactance between the antenna elements. These two are defined according to the classical induced EMF approach, following side-by-side array configuration for ULA and 2D UCA and parallel-in-echelon array configuration for 3D UCA [29], [37], and they are varied with the horizontal distance between two antennae, d_{mn}. In UCA configuration, since the antennae are placed in the circular direction, the horizontal distance between two antennae is defined as a chord length of the circle between the mth and n^{th} antennae, $d_{mn} = 2r \sin(\phi_n/2)$.

Assuming array reciprocity, the transmit and receive mutual coupling matrices are equal as $\boldsymbol{C}_t = \boldsymbol{C}_r = \boldsymbol{C}$ [36]. Due to the fact that MC coefficients between equally spaced antenna elements are the same and inversely related to their distances [38], the mutual impedance matrix can be modeled using a symmetric Toeplitz matrix as

$$\boldsymbol{Z} = \text{Toeplitz}\{z^T, z^T\}, \tag{21}$$

where $\boldsymbol{z} = [z_1, z_2, \ldots, z_N]^T \in \mathbb{C}^{N \times 1}$ is a complex vector composed of N mutual impedance values. In ULA, $\boldsymbol{z}$ can be formed by calculating Z_{1n} the mutual impedance among the first antenna and the rest of $n = 1, \ldots, N$ antennae. On the other hand, due to the symmetric structure of a circle, $\boldsymbol{z}$ in UCA structure can be reduced to

$$\boldsymbol{z} = [z_1, \ldots, z_L, z_{L-1}, \ldots, z_3, z_2], \in \mathbb{C}^{N \times 1}, \tag{22}$$

for N being an even number with $L = \frac{N}{2} + 1$, and

$$\boldsymbol{z} = [z_1, \ldots, z_L, z_L, \ldots, z_3, z_2], \in \mathbb{C}^{N \times 1}, \tag{23}$$

for N being an odd number with $L = (N + 1)/2$. Thus, it is required to only calculate $L < N$ number of mutual impedance values in UCA.

In the case of staggered 3D UCA as shown in Fig. 3, the impedance matrix can be firstly written as a block diagonal matrix of the impedance matrix of the first and the second UCA without staggered configuration, $\boldsymbol{Z}_1$ and $\boldsymbol{Z}_2$, as $\boldsymbol{Z} = \text{blkdiag}(\boldsymbol{Z}_1, \boldsymbol{Z}_2)$. Then, the upper triangular matrix of $\boldsymbol{Z}$, which consists of the mutual impedance between the antenna m of the first UCA and n of the second UCA in general, is defined by

$$\boldsymbol{Z}_u = \begin{bmatrix} Z_{1(N_1+1)} & Z_{1(N_1+2)} & . & . & Z_{1N_2} \\ Z_{2(N_1+1)} & Z_{2(N_1+2)} & . & . & Z_{2N_2} \\ . & . & . & . & . \\ . & . & . & . & . \\ Z_{N_1(N_1+1)} & Z_{N_1(N_1+2)} & . & . & Z_{N_1N_2} \end{bmatrix}, \in \mathbb{C}^{N_1 \times N_2}, \tag{24}$$

where Z_{mn}, $m = [1, \ldots, N_1]$ and $n = [N_1 + 1, \ldots, N_2]$, is calculated using EMF closed form solution based on parallel-in-echelon array configuration [29] since they are placed in staggered arrangement. Likewise, the lower triangular matrices can be obtained as $\boldsymbol{Z}_l = \boldsymbol{Z}_u^T$. Therefore, the finalized $\boldsymbol{Z}$ for Fig. 3b structure with $N_1 = 3, N_2 = 4, N = N_1 + N_2$, can be expressed by

$$\boldsymbol{Z}_u = \begin{bmatrix} \boldsymbol{Z}_1 & \boldsymbol{Z}_u \\ \boldsymbol{Z}_u^T & \boldsymbol{Z}_2 \end{bmatrix}, \in \mathbb{C}^{N \times N}. \tag{25}$$

B. ANTENNA ARRAY BEAM PATTERN IN THE PRESENCE OF MC

Considering the mutual coupling effect in the antenna array, the transmitted beam pattern, $E(\phi, \theta)$, in XY-plane has become

$$E(\phi, \theta = \pi/2) = (\boldsymbol{C}\boldsymbol{a}(\phi))^H \boldsymbol{v}(\phi_1). \tag{26}$$

In order to visualize the effect of mutual coupling, antenna patterns based on ULA, 2D UCA and 3D UCA are generated using MOM EM simulation. Without considering NOMA system, the effect of mutual coupling on the transmit beam pattern and its compensation have been discussed in [30]. Here we adopted the same antenna structures as [30], but with a larger number of antenna elements in ULA and 2D-UCA to realize highly directional beam. Fig. 4 shows the normalized farfield pattern in YZ-plane (thus, $E(\phi = \pi/2, \theta)$) steered towards the nearest user at 68°, using ULA with $d = 0.5\lambda$. Here, $\boldsymbol{v}$ is an excitation voltage vector, generated based on non-uniform amplitudes and progressive phases to direct towards the desired user. It can be seen that the maximum gain of the practical pattern with MC is reduced by 4 dB approximately as compared to 0 dB gain of the theoretical pattern without MC. After mutual coupling is compensated as discussed in [30], the resultant pattern, shown by the dashed black lines, is approximately the same as the theoretical pattern. Therefore, the loss of 4 dB can be recovered by using this technique.

Similarly, mutual coupling significantly affects the farfield beam pattern in XY-plane (thus, $E(\phi, \theta = \pi/2)$) of UCA, as depicted in Fig. 5a. Here, a UCA with $N = 8$ and
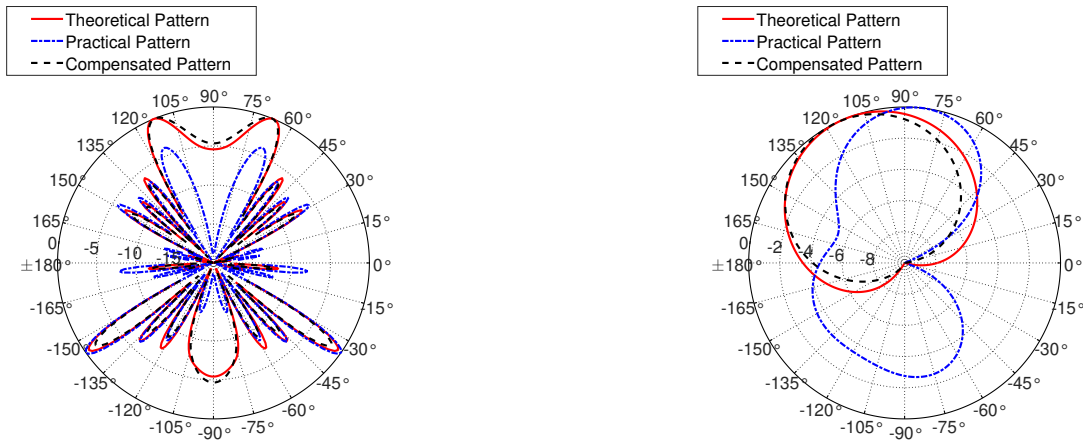
FIGURE 4. Normalized YZ-plane pattern with nearest UT-based beamformer, employing ULA with $N = 16$ and $d = 0.5\lambda$, MOM/EM simulation.

$r = 0.25\lambda$ using uniform amplitudes and progressive phases beamforming is considered. The theoretical beam, generated by nearest UT-beamforming, has the maximum gain at the desired direction $\phi_1 = 113°$, while the practical beam is shifted towards $\phi_k = 84°$, $k \neq 1$ due to MC. Again, we see that the compensated pattern is in very good agreement with the theoretical pattern in the main beam direction. Finally, we consider a 3D UCA antenna array structure in XY-plane, following the array configuration and the excitation voltages in [30], where the outer circle has $N_1 = 4$ with $r_1 = 0.5\lambda$, and the inner circle has $N_2 = 3$ with $r_2 = 0.4\lambda$ at $z = \lambda/4$. Fig 5b shows the far-field pattern for this array structure. We employ four main beams at $\phi_1 = -90°$, $\phi_2 = 0°$, $\phi_3 = 90°$ and $\phi_4 = 180°$ to target $G = 4$ groups of two-user NOMA system as a test case. The practical pattern shows a nearly 30° of beam shift from the desired direction of $\phi_1 = -90°$ and $\phi_3 = 90°$ due to MC accompanied by gain reduction. Similarly, for $\phi_2 = 0°$ there is more than 3 dB loss with unwanted side-lobe, and $\phi_4 = 180°$ has 2 dB loss in the main beam. Since such an antenna structure is widely used in BS, we can see that NOMA is nearly destroyed in this case. However, after compensating for the MC, we can see that not only the beam shift is steered back to the theoretical desired direction, but the gain reduction is also recovered.

Based on the effective steering vector, the transmitted beam power with the analog beamforming towards the nearest UT is modified as (27), and the received beam power for the kth UT at the BS after post-coding is obtained as (28) as follows

$$\zeta_{MC}^{DL}(\phi_k) = |a(\phi_k)^H C^H v|^2 = |a(\phi_k)^H C^H a(\phi_1)|^2, \quad (27)$$

$$\zeta_{MC}^{UL}(\phi_k) = |f^H C a(\phi_k)|^2 = |a(\phi_1)^H C a(\phi_k)|^2. \quad (28)$$

In the above-mentioned scenario where G number of groups are served by the BS, beams pointing to different directions are generated by hybrid beamforming, where two

(a) With UCA
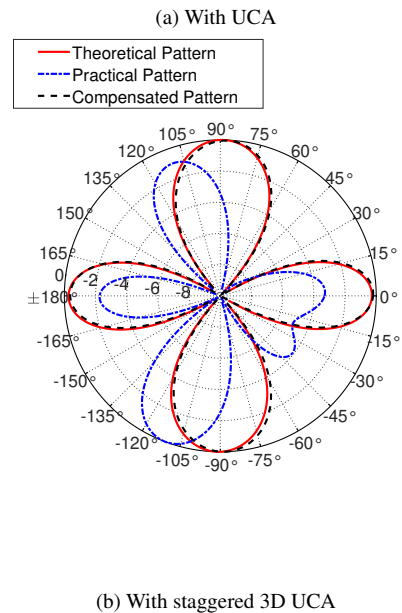

(b) With staggered 3D UCA

FIGURE 5. Normalized XY-plane pattern with nearest UT-based beamformer, employing: (a) UCA with $N = 8$ and $r = 0.25\lambda$, (b) staggered 3D UCA in XY-plane, where the outer circle has $N_1 = 4$ with $r_1 = 0.5\lambda$, and the inner circle has $N_2 = 3$ with $r_2 = 0.4\lambda$ at $z = \lambda/4$, generated by MOM/EM simulation.

UTs are supported by NOMA in each group. The channel matrix is given as $H = [h_{1_1}, h_{1_2}, \dots, h_{G_1}, h_{G_2}] \in \mathbb{C}^{N \times 2G}$. The hybrid beamforming matrix consists of steering vector-based analog beamforming with respect to the near UTs, $V_{rf} = [v_1, \dots, v_G] \in \mathbb{C}^{N \times G}$, and the baseband digital precoding matrix, which is normalized as $B_d = B_d/\sqrt{||V_{rf} B_d||_F} \in \mathbb{C}^{G \times G}$. The digital precoding is achieved by Zero-Forcing (ZF) precoding of the near UTs' effective channel matrix, $H_e = H_1^H V_{rf}$ and it is defined as $B_d = H_e^H (H_e H_e^H)^{-1}$. In the presence of MC, the coupled channel gain of the near UTs in DL transmission, resulting from the hybrid beamforming is

written by

$$U_{MC}^{near} = (CH_1)^H V_{rf} B_d \in \mathbb{C}^{G\times G}, \quad (29)$$
$$= H_1^H C^H V_{rf} H_e^H \left(H_e H_e^H\right)^{-1},$$
$$= H_1^H C^H V_{rf} V_{rf}^H H_1 \left(H_1^H V_{rf} V_{rf}^H H_1\right)^{-1}.$$

Without considering the mutual coupling matrix C, U_{MC}^{near} is a diagonal matrix, achieving zero inter-group inference between the groups. However, due the existence of the C matrix in (29), ZF based on the pre-beamforming channel is not valid, resulting in non-zero off diagonal matrix which is the inter-group inference.

C. ACHIEVABLE SUM-RATE IN THE PRESENCE OF MC

In the presence of mutual coupling, based on the coupled channel vector, the received signal at the kth UT in the downlink transmission becomes

$$y_{kMC} = \underbrace{h_k^H C^H v \sqrt{p_k} s_k}_{\text{Desired signal}} + \underbrace{\sum_{k'=1,k'\neq k}^{K} h_k^H C^H v \sqrt{p_{k'}} s_{k'}}_{\text{Interference from other users}} + w_k. \quad (30)$$

The effective achievable sum-rate of DL NOMA without compensation can be expressed as

$$\hat{R}_k^{DL} = \log_2 \left(1 + \frac{|h_k^H C^H v|^2 p_k}{\sum_{k'=1,k'\neq k}^{K} e_{k'} |h_k^H C^H v|^2 p_{k'} + \sigma_k^2}\right), \quad (31)$$

where $e_{k'} \in \{0,1\}$ is the SIC decision value based on the effective channel gain. $e_{k'} = 0$ means that there exists no interference from UT k', in other words, the signal of UT k' is decoded first and then cancelled at the UT k. On the other hand, $e_{k'} = 1$ represents the interference from UT k', hence, the signal of the UT k' is considered as noise at the UT k without decoding and cancellation process.

In multi-group NOMA system, using the hybrid beam-former of gth group, $\hat{v}_g = V_{rf} b_g$, and considering $K = 2$ UTs in each group, the effective achievable sum-rates of the near and far UTs in the presence of MC are respectively formulated as

$$\hat{R}_{g_1}^{DL} = \log_2 \left(1 + \frac{|h_{g_1}^H C^H \hat{v}_g|^2 p_1}{e_2 |h_{g_1}^H C^H \hat{v}_g|^2 p_2 + I_1 + \sigma_1^2}\right), \quad (32)$$

$$\hat{R}_{g_2}^{DL} = \log_2 \left(1 + \frac{|h_{g_2}^H C^H \hat{v}_g|^2 p_2}{e_1 |h_{g_2}^H C^H \hat{v}_g|^2 p_1 + I_2 + \sigma_2^2}\right), \quad (33)$$

where $I_k = \sum_{g'\neq g}^{G} |h_{g_k}^H C^H \hat{v}_{g'}|^2 P_{g'}$ is the inter-group interference, affecting the kth UT with total power of the group g', $P_{g'}$.

In uplink transmission, the received signal of the kth UT at the BS by considering the MC effect is given as

$$r_{kMC} = \underbrace{f^H C h_k \sqrt{p_k} s_k}_{\text{Desired signal}} + \underbrace{\sum_{k'=1,k'\neq k}^{K} f^H C h_{k'} \sqrt{p_{k'}} s_{k'}}_{\text{Interference from other users}} + f^H w. \quad (34)$$

The effective achievable sum-rate of UL NOMA without compensation can be written as

$$\hat{R}_k^{UL} = \log_2 \left(1 + \frac{|f^H C h_k|^2 p_k}{\sum_{k'=1,k'\neq k}^{K} e_{k'} |f^H C h_{k'}|^2 p_{k'} + \sigma_k^2}\right). \quad (35)$$

Assuming no mutual coupling compensation is applied in the system, hence, the analog beamforming vector is $v = a(\phi_1)$, the channel gain of the kth UT in DL transmission can be calculated according to (27) as

$$h_k = \frac{N}{\rho_k} |\alpha_k^H|^2 |a(\phi_k)^H C^H a(\phi_1)|^2. \quad (36)$$

In similar fashion, the received channel gain of the UTs in UL transmission can be obtained using the received beam power in (28).

In this study, we choose to employ analog beamforming/combining based on the steering vector of the nearest UT since we aim to avoid beamforming interference at the nearest UT for the sake of the perfect SIC operation. Based on the coupled channel gains of the UTs, we can assume the following scenarios and choose the SIC decision variable $e_{k'}$ in (31)-(33) and (35) accordingly.

1) *Case* 1 *DL*: Considering the coupled effective gain of the UTs in the following order; $\zeta_{MC}^{DL}(\phi_1) > \zeta_{MC}^{DL}(\phi_2) > \cdots > \zeta_{MC}^{DL}(\phi_K)$ with $\gamma_1 < \gamma_2 < \cdots < \gamma_K$, SIC can be performed correctly at the near users by substituting $e_{k'}$ in (31)-(33) as follows

$$e_{k'} = \begin{cases} 0, & \text{if } k' > k, \\ 1, & \text{if } k' < k. \end{cases}$$

2) *Case* 2 *DL*: In the case of significantly distorted beam pattern in Fig. 5a, assuming the farthest UT K is located at the peak direction of the distorted beam, the coupled effective gain of the UTs have become $\zeta_{MC}^{DL}(\phi_1) << \zeta_{MC}^{DL}(\phi_2) << \cdots << \zeta_{MC}^{DL}(\phi_K)$, that makes the effective channel gains, $h_1 < h_2 < \cdots < h_K$. Thus, the far users should be considered as strong users, consequently $\gamma_1 > \gamma_2 > \cdots > \gamma_K$, and SIC should be performed at the far users successively in (31)-(33), given that

$$e_{k'} = \begin{cases} 0, & \text{if } k' < k, \\ 1, & \text{if } k' > k. \end{cases}$$

However, due to unawareness of MC at the BS, the SIC operation cannot be performed at the correct UTs, resulting reduce in sum-rate.

3) *Case 3 UL*: Similar to *Case 1* and *2*, based on the effective coupled channel gain, when $\zeta_{MC}^{UL}(\phi_1) > \zeta_{MC}^{UL}(\phi_2) > \cdots > \zeta_{MC}^{UL}(\phi_K)$, SIC is correctly applied at the far UTs such that $e_{k'} = 0; \ \forall k' < k$, and $e_{k'} = 1; \ \forall k' > k$. In the presence of mutual coupling, resulting $\zeta_{MC}^{UL}(\phi_1) << \zeta_{MC}^{UL}(\phi_2) << \cdots << \zeta_{MC}^{UL}(\phi_K)$ with $h_1 < h_2 < \cdots < h_K$, SIC should be successively performed at the near UTs with $e_{k'} = 0; \ \forall k' > k$, and $e_{k'} = 1; \ \forall k' < k$ in (35).

D. MUTUAL COUPLING COMPENSATION

In the above sections we discussed three different antenna array structures for 1D, 2D, and 3D cases and showed the far-field patterns in the presence of MC respectively for the DL case. In the case, where mutual coupling is estimated perfectly and known at the BS, the modified beamforming/combining vectors can be defined as

$$\bar{v} = (C^H)^{-1} a(\phi_1), \tag{37}$$

$$\bar{f}^H = a(\phi_1)^H C^{-1}. \tag{38}$$

With mutual coupling compensated beamforming/combining vectors, the system sum-rate of the NOMA can be achieved without any loss. However, when the mutual coupling is unknown at the BS, different techniques can be applied to compensate for the mutual coupling effect. Here, we would briefly discuss the technique for MC compensation discussed in [30], which was applied to generate the compensated pattern. In general, when an antenna array is excited using a given voltage vector, v, also known as a beamforming vector, the antenna array radiates and produces a radiation pattern. This radiation pattern is distorted due to the presence of MC between antenna array elements. In order to compensate, we find a new excitation vector v' using transmission line theory such that when the array is excited with these new voltages the radiation pattern becomes equal to the theoretical pattern that assumes no MC. Thus, we are able to produce a compensated pattern that is the pattern generated in the presence of MC but is similar to our desired theoretical pattern. This technique is not only simple but also non-invasive, i.e., no physical modification is required for the antenna array structure, and only the input voltages are changed.

Similarly, in the UL case, we deal with the received voltages at the terminals of the antenna array elements. Due to the presence of MC, these received voltages are corrupted and thus results in loss of information such as in Direction Finding applications where the phase information is lost and needs to be recovered. Different techniques have been proposed for compensation in the receiving mode. A recent method in [31] for omnidirectional antennas suggests that by using a single decoupling matrix, any received voltage for all (θ, ϕ) directions can be decoupled. In other words, the mutual impedance matrix is not only constant for a given structure but is independent of the incident angle of the received signal and is only an inherent property of the structure alone. This method was further tested experimentally in [39] using Soft-ware Defined Radios (SDR). Thus, we employed the mutual coupling compensation method in [31] for the UL case.

V. NUMERICAL RESULTS

In this section, we present the numerical results of Monte Carlo simulations to evaluate the performance of NOMA system in both downlink and uplink transmission links. The simulation firstly considers the $K = 4$-user single-group NOMA system, where they are located at $d = [100, 300, 500, 1000]$ m. Then, the NOMA system with $G = 4$ groups of users with $K = 2$ UTs in each group at $d = [500, 1000]$ m, is investigated. A dominant single path channel in (1) is applied at $f_c = 2.4$ GHz with the PL exponent $\eta = 2$. The system bandwidth is 1 MHz, and the noise power density is assumed to be $N_0 = -174$ dBm/Hz. There are three scenarios in the downlink NOMA system, which are based on different array configurations; ULA, 2D-UCA, and 3D-UCA. We apply analog beamforming in ULA and 2D-UCA cases for single-group NOMA system and hybrid beamforming in 3D-UCA case for multi-group NOMA system. In all scenarios, we compare the effect of mutual coupling on the channel gains of all the UTs and the total achievable sum-rate without MC, with MC compensation, and with unknown MC. Mutual coupling generation and compensation are implemented based on the induced EMF and MOM methods in all the results. The total achievable sum-rate is calculated as a summation of the sum-rate of both users; $R_1 + R_2$, and the sum-rate results are averaged over 1000 random runs. We consider a half-wavelength dipole antenna throughout the simulation. The details of the simulation parameters are listed in Table 1.

TABLE 1. Simulation Parameters

Parameters	Value
Carrier frequency	$f_c = 2.4$ GHz
Bandwidth	1 MHz
Number of antenna at BS	ULA: $N = 16$ 2D-UCA: $N = 8$ 3D-UCA: $N_1 = 3, N_2 = 4$
Channel parameter	mmWave channel (1) with a single LOS path, $\eta = 2$
Noise power density	$N_0 = -174$ dbm/Hz
Number of UTs	Single group: $K = 4$ Multi-group: $G = 4, K = 2$ in each group
Distances	Single group: $d = [100, 300, 500, 1000]$ m Multi-group: $d = [500, 1000]$ m
Power allocation coefficients	Single group: $\gamma = [0.05, 0.15, 0.2, 0.6]$ Multi-group: $\gamma = [0.2, 0.8]$

A. UPLINK NOMA WITH ULA

Firstly we perform the simulations for uplink NOMA, where BS consisting of ULA with size $N = 16$ and $d = 0.5\lambda$. The DoA of the UTs are $\phi = [68°, 60°, 52°, 45°]$, and all UTs send the signals to the BS simultaneously in the same frequency band. Here, we assume that the users utilize the maximum transmit power available to them as $p_k = P_t/4$, where P_t is the total transmit power of the users. Figs. 6 and 7 show the received power at the BS for each user after passing through the channel. It can be observed that the MATLAB simulation

shows approximately the same results as EM simulation. In both scenarios with and without MC, the received powers at the far UTs are much lower than that of the nearest first UT since the far UTs have weak channel conditions. In the presence of MC, there is about 4 dBm decrease in the received power of the nearest UT.
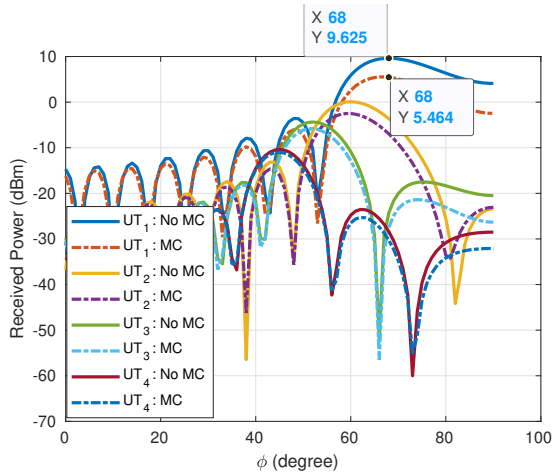
FIGURE 6. Received power for $K = 4$ UTs at the BS with the transmit power $p_k = 6.05$ dBm using EMF/MATLAB simulation.
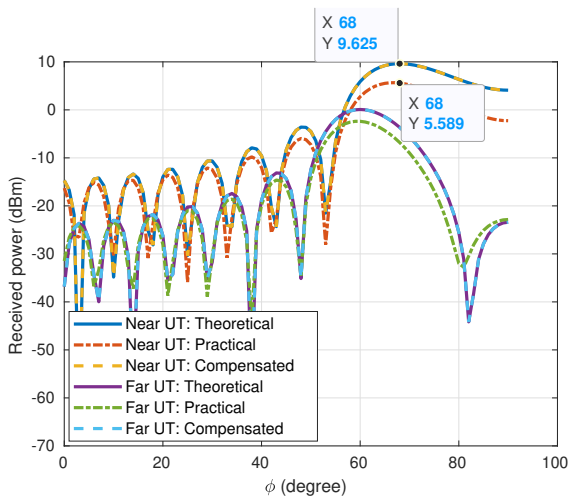
FIGURE 7. Received power for first and second UTs at the BS with the transmit power $p_k = 6.05$ dBm using MOM/EM simulation.

Fig. 8 shows the total sum-rate of the system for both theoretical without MC effect and practical with MC effect using MATLAB and EM simulations. It can be seen that the sum-rate curve without mutual coupling compensation (MC) has about 1.5 bps/Hz degradation compared to the compensated or theoretical sum-rate in both MATLAB and EM simulations.

B. DOWNLINK NOMA

In the following simulations for the downlink NOMA, we selected smaller power allocation coefficients for the nearer UTs, based on their distances from the BS, as shown in
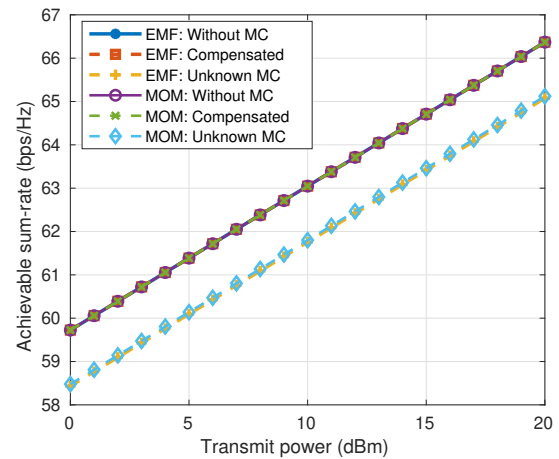
FIGURE 8. Total achievable sum-rate of uplink NOMA using ULA with $N = 16$ and $d = 0.5\lambda$.

Table 1. Three different configurations of array; ULA, UCA, and staggered 3D UCA, are implemented at the BS.

1) Downlink NOMA with ULA

In the case of ULA with $d = 0.5\lambda$ in YZ-plane ($\phi = 90°$), we assume that two users are located at $\theta = [68°, 60°]$ to demonstrate a basic NOMA system first. Fig. 9 displays the channel gain when MC affect is considered for ULA with $N = 16$ antenna, generated by EMF/MATLAB and MOM/EM simulations. In EMF/MATLAB simulation, where $v = a(\theta_1)$ is utilized, it can be seen that channel gain difference between the near UT at $\theta_1 = 68°$ and the far UT at $\theta_2 = 60°$ is around 10 dB, while in MOM/EM simulation, it is around 20 dB difference in the absence of MC. Additionally, in EM simulation with MOM, the reduce in channel gain due to mutual coupling is more significant because of its sharp drop pattern in the other directions, resulting from the non-uniform amplitudes and progress phases excitation voltages.
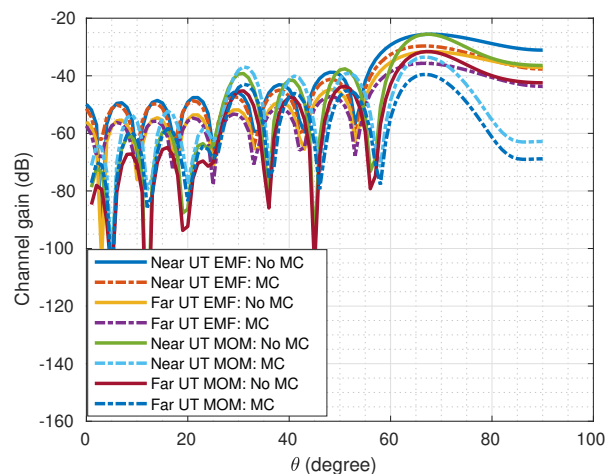
FIGURE 9. Channel gain resulting from nearest UT-based beamforming in ULA with $N = 16$, $d = 0.5\lambda$ and $\theta = [68°, 60°]$.

Then, the total achievable sum-rate of downlink NOMA system for both theoretical without MC, practical with unknown MC and with compensated MC are presented. It can be noticed from Fig. 10 that there is a difference of about 1 bps/Hz between the sum-rate curves with unknown MC for the EMF and the MOM simulations due to the different beamforming vectors. Thus, it can be summarized that the mutual coupling effect generated by MOM/EM simulation is worse than the EMF simulation with beamforming vector $v = a(\theta_1)$ due to the narrow beam generated by EM simulation using non-uniform amplitudes and progressive phases excitation voltages.

FIGURE 11. Normalized beam pattern with nearest UT-based analog beamformer $v = a(\phi_1)$, employing UCA with $N = 8$ and $r = 0.25\lambda$.

following the scenario in *Case* 1. The total achievable sum-rate is presented in Fig. 13, where there is a decrease of about 2 bps/Hz, caused by the loss in the channel gain due to mutual coupling.
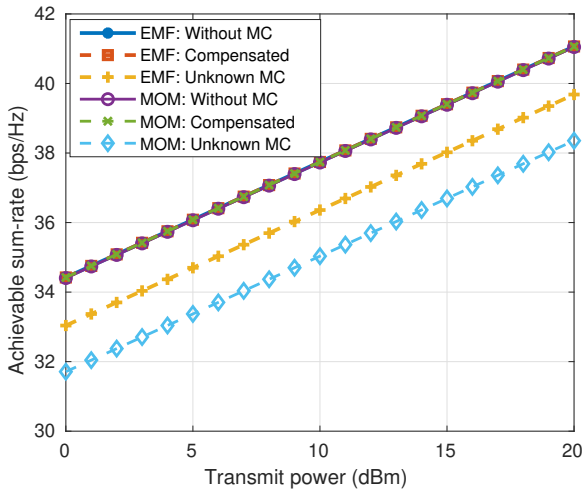

FIGURE 10. Total achievable sum-rate of downlink NOMA using ULA with $N = 16$ and $d = 0.5\lambda$.

2) Downlink NOMA with UCA

In downlink NOMA transmission where BS is equipped with one ring of UCA, we consider $K = 4$ UTs are served by a single beam. UCA with $N = 8$ and $r = 0.25\lambda$ in XY-plane ($\theta = 90°$) is employed for 2D UCA structure, and the main beam is steered to the direction of $\phi_1 = 68°$, where the nearest UT is located. The other UTs are located at $\phi = [60°, 50°, 80°]$, sequentially. Fig. 11, generated by MOM/EM simulation, illustrates the normalized transmit beam pattern based on the analog beamformer of the nearest UT, $v = a(\phi_1)$. Unlike the beam pattern of the UCA in Fig. 5a where mutual coupling distorts the direction of theoretical beam, the beam pattern with MC in Fig. 11 points the same direction as the theoretical, but with undesired back-lobe. Thus, it can be deduced that the effect of mutual coupling mainly depends on different beamforming techniques. Using the same analog beamformer of the nearest UT, Fig. 12 depicts the channel gains of $K = 4$ UTs in downlink transmission. One may observe that in the presence of MC, there is approximately 5 dB drop in the channel gains of all UTs despite having the same directivity as the channel gains without MC. Based on the channel gain differences between the near and far UTs, SIC can be performed at the near UTs,
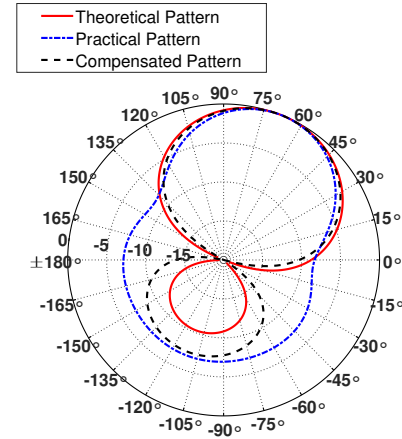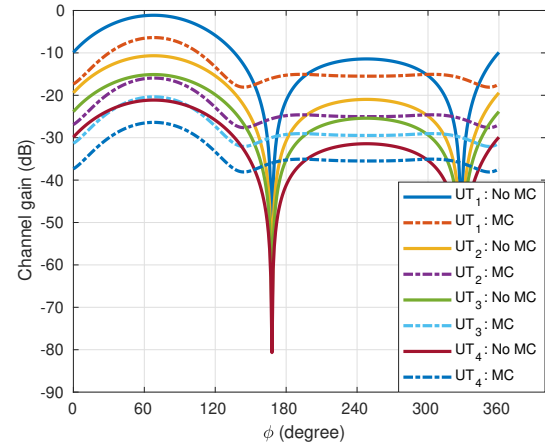

FIGURE 12. Channel gain resulting from nearest UT-based analog beamformer in UCA with $N = 8$, $r = 0.25\lambda$ and $\phi = [68°, 60°, 50°, 80°]$.

Next, we analyse the sum-rate of the NOMA system, where $K = 4$ UTs are sequentially located at different directions, $\phi = [113°, 100°, 90°, 84°]$. The effective channel gain curves based on the beam patterns generated by both MOM and EMF methods are shown in Figs. 14 and 15. It can be seen in Fig. 14 that with beamforming vector $v = a(\phi_1)$ in EMF/MATLAB simulation there is a 6 dB drop due to mutual coupling. On the other hand, based on the beam pattern in Fig. 5a generated by MOM/EM simulation when mutual coupling is considered, the peak of the effective channel gain curve is shifted to $\phi_4 = 84°$ in addition to the gain drops for all the users, as shown in Figs. 15. Thus, without considering the
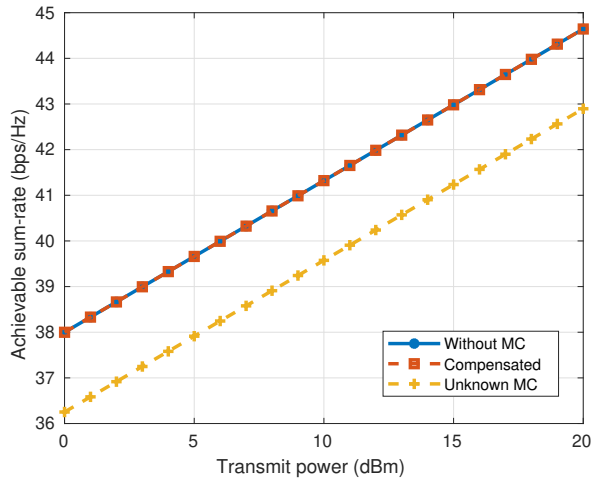
FIGURE 13. Total achievable sum-rate of downlink NOMA using UCA with $N = 8$, $r = 0.25\lambda$ and $\phi = [68°, 60°, 50°, 80°]$.

FIGURE 15. Channel gain resulting from near UT-based beamforming in UCA with $N = 8$, $d = 0.25\lambda$ and $\phi = [113°, 100°, 90°, 84°]$, generated by MOM/EMF simulation.

channel path-loss, the near UTs have lower array gain than the far UTs, making the near UTs appear to be weaker users. This is the scenario mentioned above in *Case* 2. However, due to the path-loss difference, we can see that the effective channel gains with MC of the near UTs are still greater than that of the far UTs, resulting in the *Case* 1 scenario. The total achievable sum-rate of the system based on the *Case* 1 scenario is plotted in Fig. 16. It can be observed that due to the different beamforming techniques there is a difference of about 1 ∼ 2 bps/Hz between the sum-rate curves generated by two methods in both the cases with and without MC. The sum-rate loss due to MC in MOM method is more severe than that in EMF with $\boldsymbol{v} = \boldsymbol{a}(\phi_1)$ since the practical beam pattern generated by MOM/EM simulation is more distorted and steered away to the undesired direction.
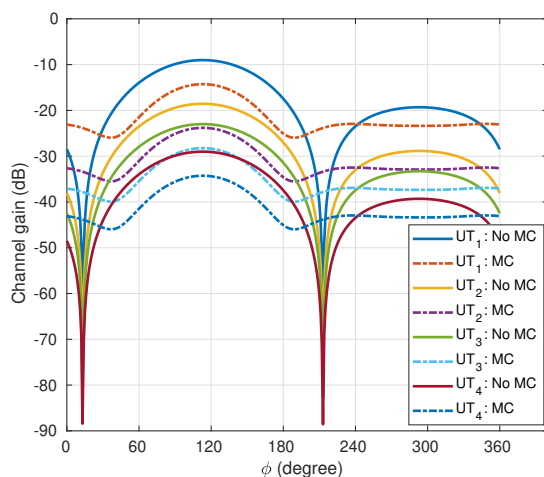

FIGURE 16. Total achievable sum-rate of downlink NOMA using UCA with $N = 8$, $r = 0.25\lambda$ and $\phi = [113°, 100°, 90°, 84°]$ for the patterns generated by MOM and EMF methods.

3) Downlink NOMA with 3-D UCA

In 5G and beyond communication systems, such as Internet-of-Things (IoT) communication, vehicular-to-everything (V2X) communication and machine-type communications (MTC) that require stable and reliable connections across all directions with massive connections, NOMA with 3D array structure can be exploited to support many users with full-directional beamforming [40] [41]. Therefore, next we implemented 3D UCA, shown in Fig. 5b, where the inner circle with $N_1 = 3$ and $r_1 = 0.4\lambda$ is located at $z = \lambda/4$ and the outer circle with $N_2 = 4$ and $r_2 = 0.5\lambda$ is placed at the origin in XY-plane. In this case, $G = 4$ number of 2-user groups are supported using 4 transmit beams generated by hybrid beamforming. $K = 8$ number of users are assumed to be located at $\phi_{g_1} = [-90°, 0°, 90°, 180°]$ with $d_1 = 500$ m for near UT and at $\phi_{g_2} = [-100°, 10°, 100°, 170°]$ with $d_2 = 1000$ m for far UT in respective group g.

Applying the combined weights of the 4 analog beamforming vector, $\boldsymbol{v} = \sum_{g=1}^{4} \boldsymbol{v}_g$, at each antenna, the resulting
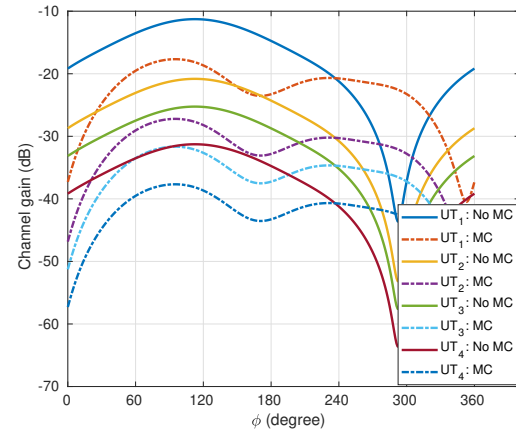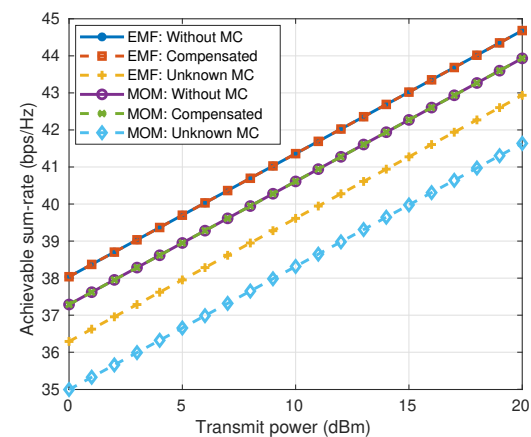

FIGURE 14. Channel gain resulting from near UT-based beamforming in UCA with $N = 8$, $d = 0.25\lambda$ and $\phi = [113°, 100°, 90°, 84°]$, generated by EMF/MATLAB simulation.

normalized beam pattern is illustrated Fig. 17, generated by MOM/EM simulation. In order to see the effect channel condition in addition to the antenna array gain, we then present the channel gain across different directions in Fig. 18, where the channel gains with MC are greatly reduced at all 3 directions except at the $\phi_4 = 180°$ due to the broadside direction. Moreover, it can be observed that the channel gains with MC at the $\phi_1 = -90°$ and $\phi_3 = 90°$ are shifted by approximately 10°. Since there is a distinct channel gain difference between the near and far users, *Case 1* scenario is considered. It is worth pointing out that digital precoding is not applied here to calculate the channel gain, but rather only the combined analog beamforming weights is utilized, thus we cannot observe the interference caused by other groups in this simulation result.
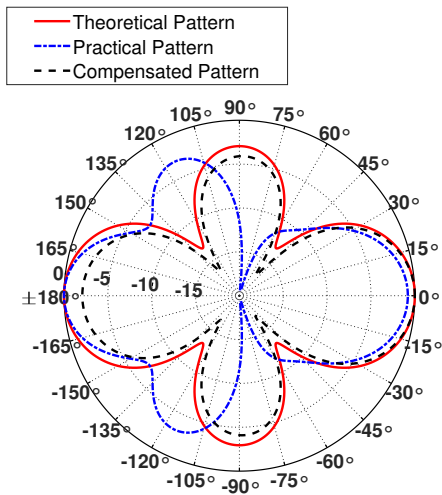

FIGURE 18. Channel gain at all the directions, using combined near UT-based analog beamforming weights, generated by EMF/MATLAB simulation.

FIGURE 19. Total achievable sum-rate of downlink NOMA using 3-D UCA.

FIGURE 17. Normalized beam pattern with the combined near UT-based analog beamforming weights using staggered 3D UCA, generated by MOM/EM simulation.

Due to the mutual coupling, interference between the group cannot be perfectly canceled by ZF as seen in (29). The ZF-based hybrid beamforming in the presence of MCM causes very high inter-group and intra-group interference, which is eventually similar to the gain at the desired direction in each group. Additionally, inter-group interference on the far user without MC is still high due to the ZF based on the near UT, while the inter-group interference on the near UT with no MC is much smaller than its channel gain. It can be seen in Fig. 19 that due the very high interference, the total achievable sum-rate of the system in the presence of MC does not benefit from the increase in transmit power and stays steady. Thus, it is essential to perfectly estimate the mutual coupling and compensate it in order to keep the system sum-rate maximum.
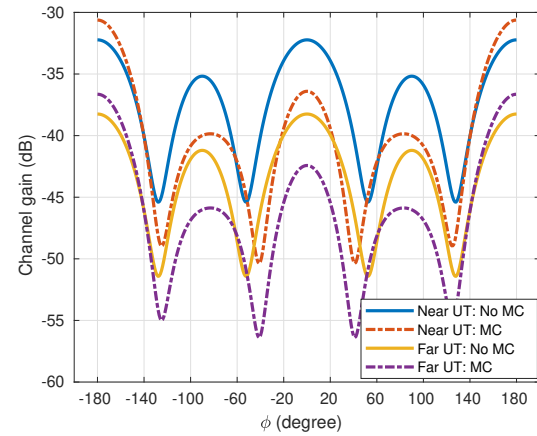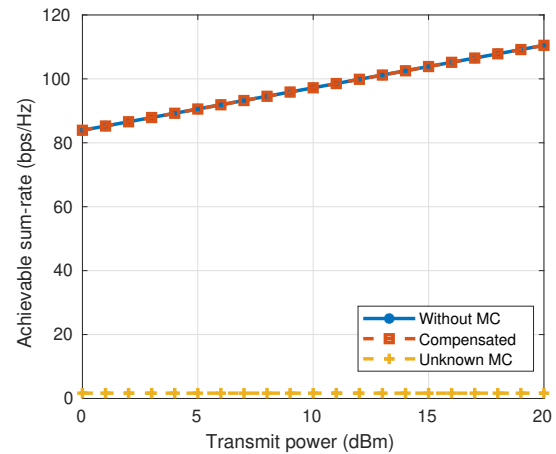
VI. CONCLUSION

In this paper, we analyzed the mutual coupling effect on the achievable sum-rate of the NOMA system in both UL and DL transmissions. A single-antenna user NOMA system with multi-antenna BS that employs analog beamforming is considered. Due to the mutual coupling between the array elements, the steering vector of the channel is undesirably affected, resulting in a distorted antenna pattern. We applied different antenna structures and configurations at the BS, such as ULA, 2D UCA, and staggered 3D UCA. MCMs are generated by using EMF and MOM approaches. We observed the effective antenna patterns and channel gains due to MC. Moreover, the modified sum-rate of the NOMA system in the presence of MC is also formulated. Based on the simulation results, it can be concluded that mutual coupling has a negative impact on the sum-rate of the NOMA system in different array structures due to a decrease in channel gain for all the users, for example, in ULA structure. In addition, mutual impedance values in UCA are larger because of the

symmetric antenna placement in a circular form. Hence, the sum-rate decrease is more significant in UCA, especially in the case with progressive phases beamforming in MOM/EM simulation owing to its shifted antenna pattern that results in a considerable drop in the desired channel gain. After observing the adverse effects of MC, matrix inversion and non-invasive compensation techniques were employed as a solution in both UL and DL to remove MC, which not only recovered the desired beam pattern but also compensated for the loss in gain. With the help of MC compensation, the effect of MC can be reduced, and thus compensation is encouraged to be applied in future applications of multi-antenna systems. Experimental verification of the multi-antenna NOMA system in the presence of mutual coupling and its compensation using SDR is considered as future work.

REFERENCES

[1] Y. Liu, Z. Qin, M. Elkashlan, Z. Ding, A. Nallanathan, and L. Hanzo, "Non-orthogonal multiple access for 5G and beyond," *Proceedings of the IEEE*, vol. 105, no. 12, pp. 2347–2381, Dec. 2017.

[2] Y. Saito, Y. Kishiyama, A. Benjebbour, T. Nakamura, A. Li, and K. Higuchi, "Non-orthogonal multiple access (NOMA) for cellular future radio access," in *Proc. IEEE 77th Veh. Technol. Conf. (VTC Spring), Dresden, Germany*. IEEE, Jun. 2013, pp. 1–5.

[3] T. Cover, "Broadcast channels," *IEEE Trans. Inf. Theory*, vol. 18, no. 1, pp. 2–14, 1972.

[4] M. Aldababsa, M. Toka, S. Gökçeli, G. K. Kurt, and O. Kucur, "A tutorial on nonorthogonal multiple access for 5G and beyond," *Wireless Commun. and Mobile Comput.*, vol. 2018, Jun. 2018.

[5] C. Kim, T. Kim, and J.-Y. Seol, "Multi-beam transmission diversity with hybrid beamforming for MIMO-OFDM systems," in *Proc. IEEE Globecom Workshops (GC Wkshps), Atlanta, GA, USA*. IEEE, Dec. 2013, pp. 61–65.

[6] B. Kim, W. Chung, S. Lim, S. Suh, J. Kwun, S. Choi, and D. Hong, "Uplink NOMA with multi-antenna," in *Proc. IEEE 81st Veh. Technol. Conf. (VTC Spring), Glasgow, Scotland*. IEEE, May 2015, pp. 1–5.

[7] S. Rangan, T. S. Rappaport, and E. Erkip, "Millimeter-wave cellular wireless networks: Potentials and challenges," *Proceedings of the IEEE*, vol. 102, no. 3, pp. 366–385, Mar. 2014.

[8] A. Ghosh, T. A. Thomas, M. C. Cudak, R. Ratasuk, P. Moorut, F. W. Vook, T. S. Rappaport, G. R. MacCartney, S. Sun, and S. Nie, "Millimeter-wave enhanced local area systems: A high-data-rate approach for future wireless networks," *IEEE J. Sel. Areas Commun.*, vol. 32, no. 6, pp. 1152–1163, Jun. 2014.

[9] L. Zhu, Z. Xiao, X.-G. Xia, and D. O. Wu, "Millimeter-wave communications with non-orthogonal multiple access for B5G/6G," *IEEE Access*, vol. 7, pp. 116 123–116 132, 2019.

[10] Z. Ding, L. Dai, R. Schober, and H. V. Poor, "NOMA meets finite resolution analog beamforming in massive MIMO and millimeter-wave networks," *IEEE Commun. Lett.*, vol. 21, no. 8, pp. 1879–1882, May 2017.

[11] Z. Xiao, L. Dai, Z. Ding, J. Choi, and P. Xia, "Millimeter-wave communication with non-orthogonal multiple access for 5G," [Online]. Available: https://arxiv.org/abs/1709.07980, 2017.

[12] S. A. R. Naqvi and S. A. Hassan, "Combining NOMA and mmWave technology for cellular communication," in *Proc. IEEE 84th Veh. Technol. Conf. (VTC-Fall), Montreal, QC, Canada*. IEEE, Sept. 2016, pp. 1–5.

[13] J. Li, X. Li, A. Wang, and N. Ye, "Performance analysis for downlink MIMO-NOMA in millimeter wave cellular network with D2D communications," *Wireless Commun. and Mobile Comput.*, vol. 2019, Jan. 2019.

[14] Y. Li, K. An, T. Liang, and W. Lu, "Sum rate of multiuser large-scale MIMO in the presence of antenna correlation and mutual coupling," *Wireless Commun. and Mobile Comput.*, vol. 2019, Jun. 2019.

[15] C. Masouros, M. Sellathurai, and T. Ratnarajah, "Large-scale MIMO transmitters in fixed physical spaces: The effect of transmit correlation and mutual coupling," *IEEE Trans. Commun.*, vol. 61, no. 7, pp. 2794–2804, May 2013.

[16] S. Henault, S. K. Podilchak, S. M. Mikki, and Y. M. Antar, "A methodology for mutual coupling estimation and compensation in antennas," *IEEE Trans. Antennas Propagat.*, vol. 61, no. 3, pp. 1119–1131, Nov. 2012.

[17] M. Wang, X. Ma, S. Yan, and C. Hao, "An autocalibration algorithm for uniform circular array with unknown mutual coupling," *IEEE Antennas Wirel. Propagat. Lett.*, vol. 15, pp. 12–15, Apr. 2016.

[18] H. Wu, C. Hou, H. Chen, W. Liu, and Q. Wang, "Direction finding and mutual coupling estimation for uniform rectangular arrays," *Elsevier Signal Process*, vol. 117, pp. 61 – 68, Dec. 2015.

[19] N. W. M. Thet, A. Kachroo, and M. K. Ozdemir, "Reduced-rank joint estimation of doa with mutual coupling," in *Proc. IEEE 26th Signal Process. Commun. App. Conf. (SIU), Izmir, Turkey*. IEEE, May 2018, pp. 1–4.

[20] ——, "Extended reduced-rank joint estimation of direction of arrival with mutual coupling for coherent signals," *Trans Emerging Telecommun. Technol.*, vol. 30, no. 12, p. e3620, Dec. 2019.

[21] H. Sajjad, S. Khan, and E. Arvas, "Mutual coupling reduction in array elements using (EBG) structures," in *Proc. Int. Appl. Comput. Electromagn. Soc. Symp. (ACES), Florence, Italy*. IEEE, Mar. 2017.

[22] P. Fletcher, M. Dean, and A. Nix, "Mutual coupling in multi-element array antennas and its influence on MIMO channel capacity," *Electronics Lett.*, vol. 39, no. 4, pp. 342–344, Feb. 2003.

[23] B. Clerckx, C. Craeye, D. Vanhoenacker-Janvier, and C. Oestges, "Impact of antenna coupling on 2×2 MIMO communications," *IEEE Trans. Veh. Technol.*, vol. 56, no. 3, pp. 1009–1018, May 2007.

[24] H. D. Nguyen, X. Wang, and H. T. Hui, "Mutual coupling and transmit correlation: Impact on the sum-rate capacity of the two-user MISO broadcast channels," in *Proc. 2011 IEEE Int. Symp. Antennas Propagat. (APSURSI), Spokane, WA, USA*. IEEE, Jul. 2011, pp. 63–66.

[25] X. Liu and M. E. Bialkowski, "Effect of antenna mutual coupling on MIMO channel estimation and capacity," *Int. J. Antennas Propagat.*, vol. 2010, Jan. 2010.

[26] S. Durrani and M. E. Bialkowski, "Effect of mutual coupling on the interference rejection capabilities of linear and circular arrays in CDMA systems," *IEEE Trans. Antennas Propagat.*, vol. 52, no. 4, pp. 1130–1134, May 2004.

[27] R. Fallahi and M. Roshandel, "Effect of mutual coupling and configuration of concentric circular array antenna on the signal-to-interference performance in CDMA systems," *Progress In Electromagn. Research*, vol. 76, pp. 427–447, 2007.

[28] S. Akkar, F. Harabi, and A. Gharsallah, "Directions of arrival estimation with planar antenna arrays in the presence of mutual coupling," *Int. J. Electronics*, vol. 100, no. 6, pp. 818–836, Jun. 2013.

[29] C. A. Balanis, *Antenna theory: analysis and design*. John wiley & sons, 2016.

[30] S. Khan, H. Sajjad, M. K. Ozdemir, and E. Arvas, "Mutual coupling compensation in transmitting arrays of thin wire antennas," *Appl. Comput. Electromagn. Soc. J. (ACES Journal)*, vol. 33, no. 11, pp. 1182–1189, Nov 2018.

[31] ——, "Mutual coupling compensation in receiving antenna arrays," in *Proc. Int. Appl. Comput. Electromagn. Soc. Symp. (ACES), Monterey, CA, USA*. IEEE, Mar. 2020.

[32] G. Lee, Y. Sung, and J. Seo, "Randomly-directional beamforming in millimeter-wave multiuser MISO downlink," *IEEE Trans. Wirel. Commun.*, vol. 15, no. 2, pp. 1086–1100, Sept. 2015.

[33] M. N. Kulkarni, A. Ghosh, and J. G. Andrews, "A comparison of MIMO techniques in downlink millimeter wave cellular networks with hybrid beamforming," *IEEE Trans. Commun.*, vol. 64, no. 5, pp. 1952–1967, Mar. 2016.

[34] B. Kim, S. Lim, H. Kim, S. Suh, J. Kwun, S. Choi, C. Lee, S. Lee, and D. Hong, "Non-orthogonal multiple access in a downlink multiuser beamforming system," in *Proc. IEEE Military Commun. Conf. (MILCOM), San Diego, California, USA*. IEEE, Nov. 2013, pp. 1278–1283.

[35] T. Svantesson, "Modeling and estimation of mutual coupling in a uniform linear array of dipoles," in *Proc. IEEE Int. Conf. Acous., Speech, Signal Process. (ICASSP99), Phoenix, AZ, USA*, vol. 5. IEEE, Mar. 1999, pp. 2961–2964.

[36] C. Zhang, H. Huang, and B. Liao, "Direction finding in MIMO radar with unknown mutual coupling," *IEEE Access*, vol. 5, pp. 4439–4447, 2017.

[37] P. Ioannides and C. A. Balanis, "Mutual coupling in adaptive circular arrays," in *Proc. IEEE Antennas Propagat. Soc. Symp., Monterey, CA, USA*, vol. 1. IEEE, Jun. 2004, pp. 403–406.

[38] B. Friedlander and A. Weiss, "Direction finding in the presence of mutual coupling," *IEEE Trans. Antennas Propagat.*, vol. 39, no. 3, pp. 273–284, Mar. 1991.

[39] S. Khan, H. Sajjad, M. K. Ozdemir, and E. Arvas, "Mutual coupling compensation in receiving arrays and its implementation on software defined

This article has been accepted for publication in a future issue of this journal, but has not been fully edited. Content may change prior to final publication. Citation information: DOI 10.1109/ACCESS.2020.3030110, IEEE Access

N. W. M. Thet *et al.*: Impact of Mutual Coupling on Power-Domain Non-orthogonal Multiple Access (NOMA)

radios," in *Proc. Int. Appl. Comput. Electromagn. Soc. Symp. (ACES), Monterey, CA, USA*. IEEE, Mar. 2020.

[40] J. Yang, W. Ryoo, W. Sung, J.-H. Kim, and J. Park, "3D antenna structures using uniform triangular arrays for efficient full-directional multiuser transmission," *Int. J Antennas Propagat.*, vol. 2019, Nov. 2019.

[41] A. Zakeri, N. Mokari, and H. Yanikomeroglu, "Joint radio resource allocation and 3D beam-forming in MISO-NOMA-based network with profit maximization for mobile virtual network operators," [Online]. Available: https://arxiv.org/abs/1907.05161, 2019.

MEHMET K. OZDEMIR received the B.S. and M.S. degrees in Electrical Engineering from Middle East Technical University, Ankara, Turkey in 1996 and 1998, respectively, and the Ph.D. degree in Electrical Engineering from Syracuse University, Syracuse, NY in 2005. Currently, he is with the Department of Electrical and Electronics Engineering, Istanbul Medipol University, Istanbul, Turkey. His research interests include channel modelling, PHY layer design, parameter estimation, and 5G massive MIMO systems.

- - -

NANN WIN MOE THET received the B.S. degree in Communication Engineering from the International Islamic University Malaysia (IIUM), KL, Malaysia in 2014, and the M.S. degree in Electronics and Computer Engineering from Istanbul Sehir University, Istanbul, Turkey in 2017. She is currently pursuing the Ph.D. degree in Electrical and Electronics Engineering with the Istanbul Medipol University, Istanbul, Turkey. Her research interests include 5G massive MIMO systems, direction estimation, beamforming, and multiple access technologies.

SANA KHAN received her B.S. degree in Engineering Sciences from Ghulam Ishaq Khan Institute (GIKI) of Engineering Sciences and Technology, Topi, KPK, Pakistan in 2013 and M.S. degree from Istanbul Medipol University, Istanbul, Turkey in August 2017. Currently, she is pursuing her Ph.D. degree in Electrical Engineering at the same university. Her research interests include computational electromagnetics, antennas, RF/MW devices, software defined radios and optical communication.

ERCUMENT ARVAS was born in 1953, in Van, Turkey. He received his B.Sc. and M.Sc. degrees in Electrical Engineering from the Middle East Technical University, Ankara, Turkey, in 1976 and 1979, respectively, and his Ph.D. degree in Electrical Engineering from Syracuse University, Syracuse, NY, USA, in 1983. From 1983 to 1984, he was with the Department of Electrical Engineering, Yildiz Technical University, Istanbul, Turkey. Between 1984 and 1987, he was with Rochester Institute of Technology, Rochester, NY, USA, and from 1987 to 2014, he was with Syracuse University. He is now teaching at the Electrical and Electronics Engineering Department, Istanbul Medipol University, Istanbul, Turkey. His research interests include electromagnetics scattering and microwave devices. Dr. Arvas is a Fellow of the Electromagnetics Academy.